

GREEN'S FUNCTION OF THE SCREENED POISSON'S EQUATION ON THE SPHERE

RAMY TANIOS, SAMAH EL MOHTAR, OMAR KNIO, AND ISSAM LAKKIS

ABSTRACT. In geophysical fluid dynamics, the screened Poisson equation appears in the shallow-water, quasi geostrophic equations. Recently, many attempts have been made to solve those equations on the sphere using different numerical methods. These include vortex methods, which solve a Poisson equation to compute the streamfunction from the (relative) vorticity. Alternatively, the streamfunction can be computed directly from potential vorticity (PV), which would offer the possibility of constructing more attractive vortex methods because PV is conserved along material trajectories in the inviscid case. On the spherical shell, however, the screened Poisson equation does not admit a known Green's function, which limits the extension of such approaches to the case of a sphere. In this paper, we derive an expression of Green's function for the screened Poisson equation on the spherical shell in series form and in integral form. A proof of convergence of the series representation is then given. As the series is slowly convergent, a robust and efficient approximation is obtained using a split form which isolates the singular behavior. The solutions are illustrated and analyzed for different values of the screening constant.

1. INTRODUCTION

In geophysical fluid dynamics, the screened Poisson equation arises in the shallow-water, quasi-geostrophic, potential vorticity equation [9, 10], for a finite Rossby radius of deformation (baroclinic case). The equation relates the streamfunction of the geostrophic flow to the potential vorticity, where the “screening” is the inverse of the Rossby radius of deformation. For an infinite Rossby radius of deformation (barotropic case), the screened Poisson equation reduces to the Poisson equation, whose Green's function is known on the spherical shell [1, 7]. Recently, many attempts using Lagrangian methods have been made to (numerically) solve the shallow-water quasi-geostrophic potential vorticity equation on the spherical shell. For instance, Bosler et al. [2] solved the barotropic vorticity (BVE) equation (infinite Rossby radius of deformation) using a Lagrangian particle/panel method. The flow field was computed from the position of particles carrying (relative) vorticity, and advecting with a velocity expressed in terms of the Biot-Savart law. However, the method did not take advantage of the conservation of potential vorticity, i.e., (relative) vorticity carried by each particle had to be updated at the new particle positions, thus requiring an additional computational cost. In [8], Mohammadian & Marshall used a vortex-in-cell (VIC) method, in which particles carried (relative)

Date: November 26, 2019.

Key words and phrases. Screened Poisson equation; shallow-water equations; sphere.

vorticity. The flow field was obtained from the streamfunction, which was computed from the vorticity by inverting a Poisson equation on an underlying Eulerian grid.

Allowing particles to carry potential vorticity enables taking advantage of the fact that potential vorticity is materially conserved in the inviscid limit. Consequently, in this case advecting/transporting particles along flow trajectories would avoid the need to integrate an evolution equation for their strengths, provided that the flow field can be immediately computed from the particle distribution. To this end, we focus on this work on deriving expressions of Green's function for the screened Poisson equation on the spherical shell.

Specifically, in section 2, we apply a spectral decomposition of the Laplace-Beltrami operator to arrive at a series representation of the Green's function. The convergence properties of this representation are then analyzed in section 3, and a computational strategy for evaluating the series is outlined in section 4. In section 5, an alternative, integral form of the Green's function is constructed. Implementation of the series and integral solutions is then illustrated in section 6, in light of results obtained for representative test cases. Concluding remarks are given in section 7.

2. DERIVATION OF GREEN'S FUNCTION

Let $\Omega = \{(\rho, \theta, \varphi) \in \mathbb{R}^+ \times [0, 2\pi] \times [0, \pi] / \rho = R\}$. Consider the screened Poisson's equation on Ω :

$$(2.1) \quad \nabla_s^2 \psi(\theta, \varphi) - \frac{1}{L_d^2} \psi(\theta, \varphi) = f(\theta, \varphi)$$

where $L_d \in \mathbb{R}^+$ is the Rossby radius of deformation and ∇_s^2 is the **Laplace-Beltrami** operator on the sphere of radius R ,

$$(2.2) \quad \nabla_s^2 = \frac{1}{R^2} \frac{1}{\sin^2 \theta} \frac{\partial^2}{\partial \varphi^2} + \frac{1}{R^2} \frac{1}{\sin \theta} \frac{\partial}{\partial \theta} (\sin \theta \frac{\partial}{\partial \theta}).$$

The spherical harmonics $Y_{l,m}(\theta, \varphi)$ form a complete basis set of the Hilbert space of all square-integrable functions, $\mathcal{H} = \{f : \Omega \rightarrow \mathbb{R} / \int_{\Omega} f^2 < \infty\}$. Thus every function in \mathcal{H} can be decomposed in terms of the mean-square convergent sum:

$$(2.3) \quad f(\theta, \varphi) = \sum_{l=0}^{\infty} \sum_{m=-l}^l f_{lm}(r) Y_{l,m}(\theta, \varphi),$$

and the solution, ψ , of (2.1) can be expressed as:

$$(2.4) \quad \psi(\theta, \varphi) = \sum_{l=0}^{\infty} \sum_{m=-l}^l u_{lm}(r) Y_{l,m}(\theta, \varphi).$$

Using the L_2 inner product:

$$(2.5) \quad \langle h(\theta, \varphi), k(\theta, \varphi) \rangle \equiv \int_{\Omega} h(\theta, \varphi) k(\theta, \varphi) dS \quad (h, k) \in \mathcal{H}^2$$

the coefficients in (2.3) are given by:

$$(2.6) \quad f_{lm} = \frac{1}{R^2} \int_{\Omega} Y_{l,m}(\theta, \varphi) f(\theta, \varphi) dS = \int_{\theta=0}^{\pi} \int_{\varphi=0}^{2\pi} Y_{l,m}(\theta, \varphi) f(\theta, \varphi) \sin \theta d\theta d\varphi.$$

Because the spherical harmonics are eigenfunctions of $\nabla_s^2|_{R=1}$ [4], that is

$$(2.7) \quad \nabla_s^2|_{R=1} Y_{l,m} = -l(l+1)Y_{l,m}$$

we have

$$(2.8) \quad \nabla_s^2 Y_{l,m} = \frac{1}{R^2} \nabla_s^2|_{R=1} Y_{l,m} = \frac{-l(l+1)}{R^2} Y_{l,m}$$

Now we write (2.1) as:

$$(2.9) \quad \sum_{l=0}^{\infty} \sum_{m=-l}^l \left[u_{lm} \frac{(-l)(l+1)}{R^2} Y_{l,m}(\theta, \varphi) - \frac{1}{L_d^2} u_{lm}(r) Y_{l,m}(\theta, \varphi) \right] = \sum_{l=0}^{\infty} \sum_{m=-l}^l f_{lm} Y_{l,m}(\theta, \varphi).$$

From the orthogonality of the basis, we obtain

$$(2.10) \quad u_{lm} = \frac{f_{lm}}{\frac{(-l)(l+1)}{R^2} - \frac{1}{L_d^2}} = \frac{\int_{\theta'=0}^{\pi} \int_{\varphi'=0}^{2\pi} Y_{l,m}(\theta', \varphi') f(\theta', \varphi') \sin \theta' d\theta' d\varphi'}{\frac{(-l)(l+1)}{R^2} - \frac{1}{L_d^2}}$$

and

$$(2.11) \quad \begin{aligned} \psi(\theta, \varphi) &= \sum_{l=0}^{\infty} \sum_{m=-l}^l \frac{f_{lm}}{\frac{(-l)(l+1)}{R^2} - \frac{1}{L_d^2}} Y_{l,m}(\theta, \varphi) \\ &= \sum_{l=0}^{\infty} \sum_{m=-l}^l \frac{\int_{\theta'=0}^{\pi} \int_{\varphi'=0}^{2\pi} Y_{l,m}(\theta', \varphi') f(\theta', \varphi') \sin \theta' d\theta' d\varphi'}{\frac{(-l)(l+1)}{R^2} - \frac{1}{L_d^2}} Y_{l,m}(\theta, \varphi) \end{aligned}$$

$$(2.13) \quad = \int_{\theta'=0}^{\pi} \int_{\varphi'=0}^{2\pi} \sum_{l=0}^{\infty} \sum_{m=-l}^l \frac{Y_{l,m}(\theta, \varphi) Y_{l,m}(\theta', \varphi')}{(-l)(l+1) - \frac{R^2}{L_d^2}} f(\theta', \varphi') R^2 \sin \theta' d\theta' d\varphi'$$

Because $\psi = G * f$, we have:

$$(2.14) \quad G((R, \theta, \varphi), (R, \theta', \varphi')) = \sum_{l=0}^{\infty} \sum_{m=-l}^l \frac{Y_{l,m}(\theta', \varphi') Y_{l,m}(\theta, \varphi)}{(-l)(l+1) - \frac{R^2}{L_d^2}}$$

$$(2.15) \quad = \sum_{l=0}^{\infty} \frac{1}{(-l)(l+1) - \frac{R^2}{L_d^2}} \sum_{m=-l}^l Y_{l,m}(\theta', \varphi') Y_{l,m}(\theta, \varphi)$$

Using (i) the spherical harmonics addition theorem [4]:

$$(2.16) \quad \forall (R, \theta, \varphi), (R, \theta', \varphi') \in \Omega, \quad \frac{4\pi}{2l+1} \sum_{m=-l}^l Y_{l,m}(\theta, \varphi) Y_{l,m}(\theta', \varphi') = P_l(\cos \gamma)$$

where γ is the angle at the center between (R, θ, φ) and (R, θ', φ') , and (ii) the identity $\cos \gamma = \cos \theta \cos \theta' + \sin \theta \sin \theta' \cos(\varphi - \varphi')$, we obtain

$$(2.17) \quad G((R, \theta, \varphi), (R, \theta', \varphi')) = \sum_{l=0}^{\infty} \frac{1}{(-l)(l+1) - \frac{R^2}{L_d^2}} \frac{2l+1}{4\pi} P_l(\cos(\gamma))$$

$$(2.18) \quad = \boxed{\frac{-1}{4\pi} \sum_{l=0}^{\infty} \frac{2l+1}{l(l+1) + \frac{R^2}{L_d^2}} P_l(\cos(\gamma))}$$

3. CONVERGENCE OF THE SERIES REPRESENTATION

In this section, we briefly examine properties of the Green's function series representation. To this end, we study the behavior of:

$$(3.1) \quad f(w, \gamma) = \sum_{l \geq 0} \frac{(2l+1) P_l(\cos(\gamma))}{l(l+1)+w}, \quad w \in \mathbb{R}^+.$$

For $\cos(\gamma) = 1$, we have $P_l(\cos(\gamma)) = 1$, $\forall l \in \mathbb{N}$, consequently

$$(3.2) \quad \sum_{l \geq 0} \frac{2l+1}{l(l+1)+w} \sim \sum_{l \geq 0} \frac{2}{l+w},$$

and so the series diverges like the harmonic series.

For $\cos(\gamma) \neq 1$, we have

$$(3.3) \quad f(w, \gamma) = 2 \sum_{l \geq 0} \frac{l P_l(\cos(\gamma))}{l(l+1)+w} + \sum_{l \geq 0} \frac{P_l(\cos(\gamma))}{l(l+1)+w}.$$

The second series is absolutely convergent because

$$(3.4) \quad \sum_{l \geq 0} \left| \frac{P_l(\cos(\gamma))}{l(l+1)+w} \right| \leq \sum_{l \geq 0} \frac{1}{l^2+w} < \infty, \quad \forall w \in \mathbb{R}^+$$

Now consider the first series, let $A_l = \frac{l}{l(l+1)+w}$ and $B_l = P_l(\cos(\gamma))$. Clearly, $A_l \geq 0$ and $\lim_{l \rightarrow \infty} A_l = 0$. Hence, there exists $l^* \in \mathbb{N}$ such that $A_{l+1} \leq A_l$ for all $l \geq l^*$. We now rewrite the first series on the right hand side of (3.3) as:

$$(3.5) \quad \underbrace{\sum_{l=0}^{l^*} \frac{l P_l(\cos(\gamma))}{l(l+1)+w}}_{\text{finite sum}} + \sum_{k=0}^{\infty} \frac{(l^*+k+1) P_{(l^*+k+1)}(\cos(\gamma))}{(l^*+k+1)((l^*+k+2))+w}.$$

Let us show that the second member is convergent using the Dirichlet Test. We have already shown that $A_l \rightarrow 0$ and that it is monotonically decreasing for $l \geq l^*$. It remains to show that there exists $M \geq 0$ such that $\left| \sum_{l=0}^N P_l(\cos(\gamma)) \right| \leq M$ for all N .

Note that if $\cos(\gamma) = -1.0$, the $P_l(\cos(\gamma)) = (-1)^l P_l(1) = (-1)^l$, therefore $\sum_{l=0}^N P_l(\cos(\gamma)) = \pm 1$, which is bounded.

We may thus assume that $|\cos(\gamma)| < 1$. We make use of (i) the Legendre generating function:

$$(3.6) \quad \sum_{l=0}^{\infty} u^l P_l(y) = \frac{1}{\sqrt{u^2 - 2yu + 1}},$$

with $y = \cos(\gamma)$, and (ii) the binomial series expansion $(1+x)^{1/2}$ with $x = u^2 - 2y$.

For $0 < \cos(\gamma) < 1$, we let $u = 1$, so we have $x = 1 - 2\cos(\gamma) < 1$. Consequently, the binomial series converges and the Legendre sum is bounded. For $-1 < \cos(\gamma) < 0$, we use the fact that $P_l(-\cos(\gamma)) = (-1)^l P_l(\cos(\gamma))$, let $u = -1$ and $x = 1 - 2|\cos(\gamma)|$. Following the same argument as before, we conclude that the sum is bounded. Finally, if $\cos(\gamma) = 0$, we may set $u \pm 1$, which leads $x = 1$, and the same conclusion as before.

Consequently, by the Dirichlet test, the series $\sum_{l=0}^{\infty} \frac{l P_l(\cos(\gamma))}{l(l+1)+w}$ converges when $\cos(\gamma) < 1$.

4. NUMERICAL APPROXIMATION OF THE SERIES REPRESENTATION

In the tests below, we assess two approaches for estimating the Green's function based on its series representation. The first is a straightforward approach based on truncating (2.18) at a suitably large index, l' , namely through:

$$(4.1) \quad G((R, \theta, \varphi), (R, \theta', \varphi')) \approx \frac{-1}{4\pi} \sum_{l=0}^{l'} \frac{2l+1}{(l)(l+1) + \frac{R^2}{L_d^2}} P_l(\cos(\gamma)).$$

We refer to (4.1) as the truncated approximation.

A second, alternative approach is developed based on first splitting (2.18) according to:

$$(4.2) \quad G((R, \theta, \varphi), (R, \theta', \varphi')) = \frac{-1}{4\pi R^2} \sum_{l=0}^{l'-1} \frac{2l+1}{\frac{l(l+1)}{R^2} + \frac{1}{L_d^2}} P_l(\cos(\gamma)) + \frac{-1}{4\pi R^2} \sum_{l=l'}^{\infty} \frac{2l+1}{\frac{l(l+1)}{R^2} + \frac{1}{L_d^2}} P_l(\cos(\gamma)).$$

Selecting l' such that $\frac{l'(l'+1)}{R^2} \gg \frac{1}{L_d^2}$, we may approximate G according to:

$$(4.3) \quad G((R, \theta, \varphi), (R, \theta', \varphi')) \approx \frac{-1}{4\pi R^2} \sum_{l=0}^{l'-1} \frac{2l+1}{\frac{l(l+1)}{R^2} + \frac{1}{L_d^2}} P_l(\cos(\gamma)) + \frac{-1}{4\pi R^2} \sum_{l=l'}^{\infty} \frac{2l+1}{\frac{l(l+1)}{R^2}} P_l(\cos(\gamma)).$$

Let

$$(4.4) \quad G^*((\theta, \varphi), (\theta', \varphi')) = \frac{1}{4\pi} \log\left(\frac{e}{2}(1 - \cos(\gamma))\right)$$

denote the Green's function of the Poisson equation on the sphere,

$$(4.5) \quad \nabla_s^2 \psi(\theta, \varphi) = f(\theta, \varphi).$$

G^* can be expressed in series form as:

$$(4.6) \quad G^*((\theta, \varphi), (\theta', \varphi')) = \frac{-1}{4\pi} \sum_{l=1}^{\infty} \frac{2l+1}{(l)(l+1)} P_l(\cos(\gamma))$$

Inserting (4.6) into (4.3) and rearranging we finally obtain:

$$(4.7) \quad \begin{aligned} G((R, \theta, \varphi), (R, \theta', \varphi')) &\approx -\frac{L_d^2}{4\pi R^2} - \frac{1}{4\pi R^2} \sum_{l=1}^{l'-1} \left[\frac{2l+1}{\frac{(l)(l+1)}{R^2} + \frac{1}{L_d^2}} - \frac{2l+1}{\frac{(l)(l+1)}{R^2}} \right] P_l(\cos(\gamma)) \\ &+ \frac{1}{4\pi} \log\left(\frac{e}{2}(1 - \cos(\gamma))\right), \end{aligned}$$

which we refer to as the split approximation. Because the Rossby radius, L_d , defines a distance on the circumference of the sphere, and the distance between the source and target on the sphere is $R\gamma$, we introduce the characteristic angle of the problem $\gamma^* \equiv L_d/R$. The Green's function and its split sum approximation are then expressed in terms of γ^* as:

$$(4.8) \quad \begin{aligned} G(\gamma, \gamma^*) \approx G_{l'}(\gamma, \gamma^*) &= -\frac{\gamma^{*2}}{4\pi} - \frac{1}{4\pi} \sum_{l=1}^{l'-1} \left[\frac{2l+1}{(l)(l+1) + \frac{1}{\gamma^{*2}}} - \frac{2l+1}{(l)(l+1)} \right] P_l(\cos(\gamma)) \\ &+ \frac{1}{4\pi} \log\left(\frac{e}{2}(1 - \cos(\gamma))\right). \end{aligned}$$

As further discussed below, with the same truncation index, l' , the split approximation leads to estimates exhibiting appreciably smaller relative errors than straightforward truncation. It also exhibits faster and more robust convergence as l' increases.

5. INTEGRAL FORM

In this section, we exploit the series solution (2.18) to derive an alternative, integral form of the Green's function. To this end, we make use of the following identity,

$$(5.1) \quad \frac{1}{l+R} = \int_0^{+\infty} e^{-z(l+R)} dz, \quad \operatorname{Re}(l+R) > 0,$$

and factor term $l(l+1) + \frac{R^2}{L_d^2}$ as $(l-S_1)(l-S_2)$ where $S_1, S_2 \in \mathbb{C}$.

We then perform the partial fraction expansion,

$$\frac{2l+1}{l(l+1) + \frac{R^2}{L_d^2}} = \frac{s_1}{l-S_1} + \frac{s_2}{l-S_2},$$

where $s_1, s_2 \in \mathbb{C}$. Note that S_1 and S_2 are complex conjugates that are independent of l , and so are s_1 and s_2 .

Next, we apply (5.1) to re-express the fractions $s_1/(l-S_1)$ and $s_2/(l-S_2)$ respectively according to:

$$\frac{s_1}{l-S_1} = s_1 \int_0^{+\infty} e^{-z(l-S_1)} dz,$$

and

$$\frac{s_2}{l-S_2} = s_2 \int_0^{+\infty} e^{-z(l-S_2)} dz.$$

Substituting these representations into (2.18), we get:

$$(5.2) \quad G(R, \theta, \phi) = \frac{-1}{4\pi} \sum_{l=0}^{\infty} \left(\int_0^{+\infty} s_1 e^{-z(l-S_1)} + s_2 e^{-z(l-S_2)} dz \right) P_l(\cos(\gamma))$$

$$(5.3) \quad = \frac{-1}{4\pi} \sum_{l=0}^{\infty} \left(\int_0^{+\infty} e^{-zl} [s_1 e^{zS_1} + s_2 e^{zS_2}] dz \right) P_l(\cos(\gamma))$$

$$(5.4) \quad = \frac{-1}{4\pi} \int_0^{+\infty} (s_1 e^{zS_1} + s_2 e^{zS_2}) \sum_{l=0}^{\infty} (e^{-z})^l P_l(\cos(\gamma)) dz.$$

Finally, we use the Legendre generating function to re-express the summation in (5.4), which results in:

$$(5.5) \quad G(R, \theta, \phi) = \frac{-1}{4\pi} \int_0^{+\infty} \frac{(s_1 e^{zS_1} + s_2 e^{zS_2})}{\sqrt{e^{-2z} - 2e^{-z} \cos(\gamma) + 1}} dz.$$

A more convenient form of (5.5) can be obtained by substituting the values of S_1, S_2, s_1 and s_2 , namely $s_1 = s_2 = 1$, and

$$S_1 = -\frac{1}{2} + i\beta, \quad S_2 = -\frac{1}{2} - i\beta,$$

where

$$\beta \equiv \sqrt{\frac{R^2}{L_d^2} - \frac{1}{4}}.$$

Performing the substitution and rearranging, we obtain:

$$(5.6) \quad G(R, \theta, \phi) = \frac{-1}{2\pi} \int_0^{+\infty} \frac{e^{-z/2} \cos(\beta z)}{\sqrt{e^{-2z} - 2e^{-z} \cos(\gamma) + 1}} dz.$$

Below, we use a quadrature approximation of (5.6) to verify results obtained using the series representation.

Note that for particular values of $\cos(\gamma)$, the integral in (5.6) can be evaluated analytically with the result expressed in terms of elementary functions. Specifically, for $\cos(\gamma) = -1$, we have (see [6], article 3.981):

$$(5.7) \quad G|_{\cos(\gamma)=-1} = \frac{-1}{4 \cosh(\pi\beta)}$$

whereas for $\cos(\gamma) = 0$ we obtain (see [6], article 3.985):

$$(5.8) \quad G|_{\cos(\gamma)=0} = \frac{-1}{8\pi^{3/2}} \Gamma\left(\frac{1}{4} + i\frac{\beta}{2}\right) \Gamma\left(\frac{1}{4} - i\frac{\beta}{2}\right)$$

where Γ denotes the gamma function. In particular, we use the results to verify both our quadrature and series approximations.

Also note the integral representation in (5.6) can alternatively be expressed in terms of associated Legendre function, namely according to:

$$(5.9) \quad G(R, \theta, \phi) = -\frac{1}{4 \cosh(\pi\beta)} P_{-\frac{1}{2}+i\beta}(\cos(\pi - \gamma))$$

Because the zeros of $P_{-\frac{1}{2}+i\beta}(z)$ are all real and greater than unity (see [6], article 8.784), we conclude that $G(R, \theta, \phi)$ is negative in the entire range $0 < \gamma \leq \pi$ whereas it diverges to $-\infty$ as $\gamma \rightarrow 0$.

6. RESULTS

In this section, we first compare the split sum to the direct sum in terms of their behavior as a function of the number of terms, for the case $L_d = 1000$ km. The computations are carried out in Fortran using quadruple precision for real numbers and double precision for integers. Second, we show the absolute error versus the number of terms for the split sum approximation, for $L_d = 100$ km and $L_d = 1000$ km. These two values are selected to represent the low and high values of the Rossby radius of deformation in the ocean and the atmosphere[5, 3]. Third, we compare, for $L_d = 1000$ km, the values of the Green's function computed using the split sum approximation to those computed using the high precision Numerical Integration Polyalgorithm of MapleTM. Fourth, we present plots, for different values of L_d , of the Green's function computed using the split sum versus the angle. Finally, tables of the Green's function versus the angle for different values of L_d are also presented in the appendix.

Figure 1 depicts the estimates obtained using the split sum and the direct sum as a function of the number of terms retained in the corresponding expansions. Two cases are considered, namely $\cos(\gamma) = -1.0$ and $\cos(\gamma) = 0.9$. The first case corresponds to a maximum separation between the target and the source. In the second case, the angle separating the target from the source is small. In both cases

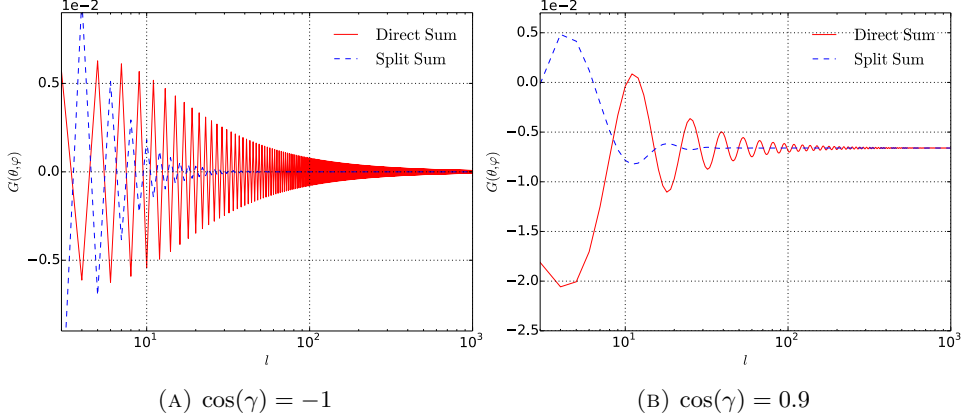


FIGURE 1. $G(\theta, \varphi)$ versus the number of terms for (a) $\cos(\gamma) = -1$, (b) $\cos(\gamma) = 0.9$. Curves are generated for $L_d = 1000$ km using the direct and split sum as indicated.

$L_d = 1000$ km. We observe from Figures 4a and 4b that the split sum converges faster than the direct sum. One can also observe that the rate of convergence is slower for $\cos(\gamma) = -1.0$. In fact, for a given value of L_d , the rate of convergence of the split sum is the slowest when $\cos(\gamma) = -1.0$. This is because the Legendre polynomial in the split sum approximation of equation (4.7) switches sign every term, i.e. $P_l(-1)P_{l+1}(-1) < 0$.

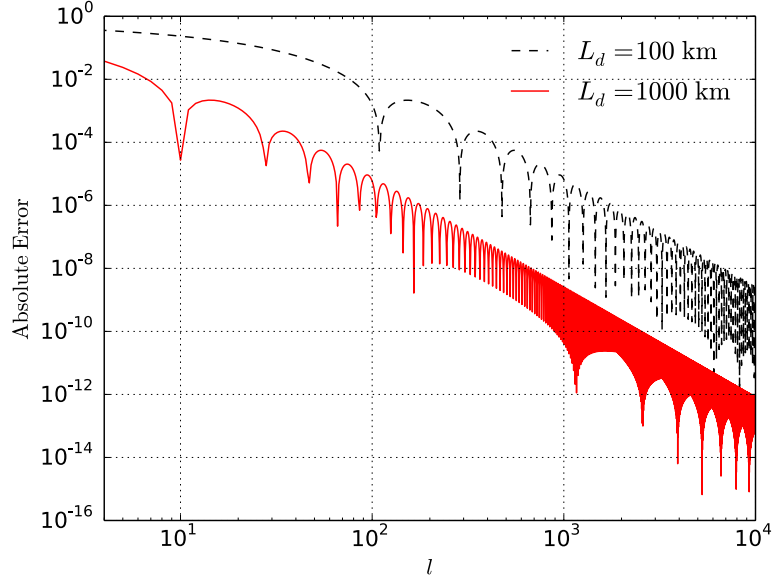


FIGURE 2. The absolute error (Eq. 6.1) versus the number of terms for $\gamma = \gamma^*$. Curves are generated using the split sum, for $L_d = 1000$ km and 100 km as indicated.

Figure 2 shows the absolute error of the split sum estimate versus the number of terms at $\frac{\gamma}{\gamma^*} = 1$, for $L_d = 1000$ km and $L_d = 100$ km. The absolute error is computed as

$$(6.1) \quad E(l) = \left| \hat{G}(\gamma, \gamma^*) - G_l(\gamma, \gamma^*) \right|,$$

where the “converged” solution \hat{G} is the value of G obtained after a sufficiently large number of terms, l' , is used in the summation, such that the coefficient multiplying the Legendre polynomial in the l' th term of the split sum is within quadruple machine precision. (Actually, it may be shown that for a desired cutoff value of this coefficient, ϵ , the number of terms needed is $l' \simeq \sqrt[3]{\frac{2}{\epsilon\gamma^{*2}}}$.) It can be observed that the asymptotic rate of convergence for both values of L_d appears to be similar (~ -3.5 on the log-log plot), though evidently a larger number of terms must be included as L_d decreases. Note that $\hat{G}(\gamma, \gamma^*)$ is in close agreement with the value computed using the Numerical Integration Polyalgorithm of Maple™ to within 16 decimal points, which is the precision of the Maple integration, as can be seen in Table 1. Table 1 shows that the split sum approximation matches the numerical integration using the Numerical Integration Polyalgorithm of Maple™ over the range $0.001 \leq \frac{\gamma}{\gamma^*} \leq 10$ for $L_d = 1000$ km ($\gamma^* = 0.15696123$). The agreement improves from 8 significant digits at $\frac{\gamma}{\gamma^*} = 0.001$ to 16 significant digits at $\frac{\gamma}{\gamma^*} = 10$. For the cases $\cos(\gamma) = 0$ and $\cos(\gamma) = -1$, the split sum approximation matches the closed form solutions (5.8) and (5.7), as shown in Table 2 for different values of L_d .

Equation (4.8) can be expressed as

$$(6.2) \quad G_{l'}(\gamma, \gamma^*) = -\frac{\gamma^{*2}}{4\pi} - \frac{1}{4\pi} \sum_{l=1}^{l'-1} \left[\frac{2l+1}{(l)(l+1) + \frac{1}{\gamma^{*2}}} - \frac{2l+1}{(l)(l+1)} \right] P_l(\cos(\gamma)) + G^*(\gamma),$$

where $G^*(\gamma) = \frac{1}{4\pi} \log\left(\frac{e}{2}(1 - \cos(\gamma))\right)$ is the Green's function of Poisson's equation on the sphere, without the screening term. To explore the departure of G from G^* , plots of $(G - G^*)(\gamma, \gamma^*)$ and $-G^*(\gamma, \gamma^*)$ versus γ/γ^* are presented in Figure 3 for the range $50 \text{ km} \leq L_d \leq 1000 \text{ km}$.

It can be observed from figure 3 that for sufficiently large γ/γ^* , the $-G^*$ curve collapses onto the $G - G^*$ curve, indicating that the Green's function of the screened Poisson equation decays at a much faster rate than that of the Poisson equation. This is attributed to the role of the screening term ψ/L_d^2 in localizing the solution to a neighborhood of the order γ^* . This can also be seen in Figures 4a and 4b, where G , G^* , and $G - G^*$ are plotted versus γ/γ^* for $L_d = 50$ km and $L_d = 1000$ km, respectively. It can be observed that G becomes increasingly localized on the sphere as L_d decreases. As such, a compact approximation of G for small values of L_d may prove suitable.

7. CONCLUSIONS

In this paper, analytical expressions are derived of the Green's function of the screened Poisson's equation on the sphere, namely in the form of an integral representation and of a series solution involving Legendre polynomials. A robust and efficient numerical approximation of the series representation is then developed.

TABLE 1. The integral approximation of the Green's function using the Numerical Integration Polyalgorithm of MapleTM and the split sum approximation for $L_d = 1000$ km ($\gamma^* = 0.15696123$). The stopping criterion used for the split sum is when the absolute value of the factor multiplying the Legendre polynomial reaches quadruple machine precision. Except for the first two entries, the Maple integral was calculated to 16 significant digits. For $\gamma/\gamma^* = 0.001$, the maximum number of digits attained was 12 whereas for $\gamma/\gamma^* = 0.005$, it was 15 digits.

γ/γ^*	Maple	Split Sum
0.001	-1.11851154768	-1.1185115466790030
0.005	-0.862367611582155	-0.86236761566019138
0.01	-0.7520661831497065	-0.75206618670609104
0.02	-0.6418055952187355	-0.64180559877292642
0.03	-0.5773592542889705	-0.57735925783975817
0.04	-0.5316835690653312	-0.53168357261181198
0.05	-0.4963020973589550	-0.49630209499805700
0.06	-0.4674384556430355	-0.46743845917847821
0.07	-0.4430777083432368	-0.44307770767107485
0.08	-0.4220167638214708	-0.42201676734310684
0.09	-0.4034793378064005	-0.40347933155959809
0.1	-0.3869351828355970	-0.38693518049861692
0.15	-0.3237421092103450	-0.32374210306526552
0.2	-0.2796019048871758	-0.27960190262165774
0.25	-0.2459853828209132	-0.24598538282091331
0.3	-0.2190766246998643	-0.21907661890074209
0.4	-0.1780154655314450	-0.17801546345860769
0.5	-0.1477460718583630	-0.14774607185836305
0.6	-0.1243523124660145	-0.12435230751870802
0.7	-0.1057148171283462	-0.10571481912301701
0.8	-9.055025072697948E-002	-9.0550249089805523E-002
0.9	-7.801957852946700E-002	-7.8019581252887993E-002
1	-6.754292534703262E-002	-6.7542925347032642E-002
2	-1.846304821245086E-002	-1.8463048212450855E-002
3	-5.714300085292792E-003	-5.7143000852927931E-003
4	-1.870693766774068E-003	-1.8706937667740684E-003
5	-6.333928838453482E-004	-6.3339288384534867E-004
6	-2.195637338314424E-004	-2.1956373383144240E-004
7	-7.750693244142898E-005	-7.7506932441429000E-005
8	-2.777791606780832E-005	-2.7777916067808478E-005
9	-1.009014887236524E-005	-1.0090148872365168E-005
10	-3.711685976274890E-006	-3.7116859762750061E-006

TABLE 2. The split sum approximation for $\gamma = \pi/2$ and π compared to Equations (5.8) and (5.7).

L_d (km)	Split Sum ($\cos(\gamma) = 0$)	Equation (5.8)
300	-1.4225814713795086E-016	-1.4225594675545431E-0016
400	-6.8995961107067088E-013	-6.8995960864883886E-0013
500	-1.1530544611076218E-010	-1.1530544610815334E-0010
600	-3.5617983195546507E-009	-3.5617983195574219E-009
700	-4.1828668580602192E-008	-4.1828668580605125E-008
800	-2.6799479475630453E-007	-2.6799479475630768E-007
900	-1.1452992927108748E-006	-1.1452992927108717E-006
1000	-3.6839641135260536E-006	-3.6839641135260568E-006
1100	-9.6329029580597044E-006	-9.6329029580597082E-006
1200	-2.1556389233382265E-005	-2.1556389233382263E-005
1300	-4.2781705365952404E-005	-4.2781705365952408E-005
1400	-7.7247341254381796E-005	-7.7247341254381793E-005
1500	-1.2929790801598909E-004	-1.2929790801598909E-004
1600	-2.0346827424618137E-004	-2.0346827424618136E-004
1700	-3.0428682816304554E-004	-3.0428682816304552E-004
1800	-4.3611425145919584E-004	-4.3611425145919584E-004
1900	-6.0302349401310045E-004	-6.0302349401310041E-004
2000	-8.0871962518105109E-004	-8.0871962518105106E-004
L_d (km)	Split Sum ($\cos(\gamma) = -1$)	Equation (5.7)
600	-1.6930096452253692E-015	-1.6890307829549300E-015
700	-1.9949869771970800E-013	-1.9950267658105915E-013
800	-7.1590372634355031E-012	-7.1590332845768866E-012
900	-1.1609776217297870E-010	-1.1609776615183131E-010
1000	-1.0797889438705467E-009	-1.0797889398916860E-009
1100	-6.7027265321956257E-009	-6.7027265361744720E-009
1200	-3.0722971586707354E-008	-3.0722971582728503E-008
1300	-1.1152376939660639E-007	-1.1152376939262755E-007
1400	-3.3703407951899458E-007	-3.3703407952297341E-007
1500	-8.7963567819438533E-007	-8.7963567819836426E-007
1600	-2.0379565833152491E-006	-2.0379565833112706E-006
1700	-4.2803676572173898E-006	-4.2803676572213691E-006
1800	-8.2844410488393729E-006	-8.2844410488353935E-006
1900	-1.4967463004072891E-005	-1.4967463004068912E-005
2000	-2.5504778524850583E-005	-2.5504778524854560E-005

This approximation is based on a splitting of the series representation that is tailored to isolate the singular behavior. Efficiency and robustness of the split series approximation was established by showing the rapid decay of the truncation error with the number of terms, and by comparing estimates with results obtained using high precision numerical integration. The solutions presented, in both graph and tabular forms, for different values of the normalized screening constant versus the normalized angle provide an effective means for accurate evaluation of the Green's function.

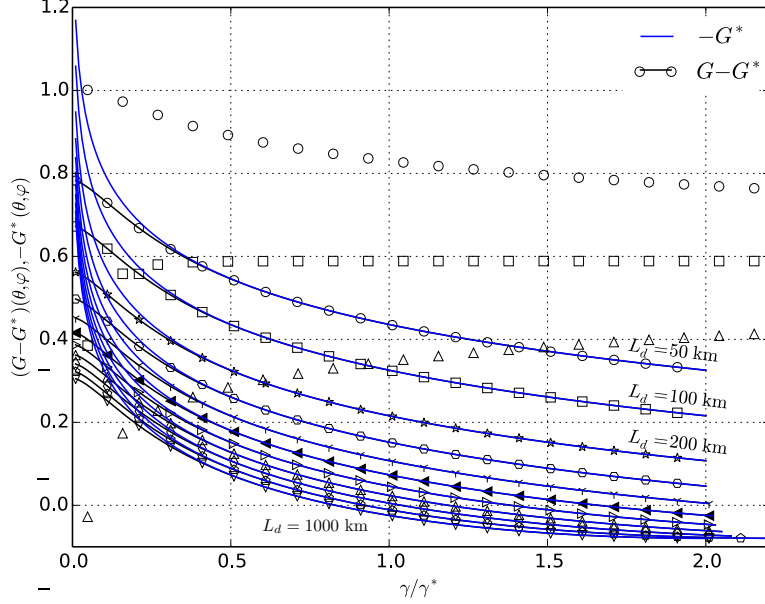


FIGURE 3. $(G - G^*)$ and $-G^*$ vs. γ/γ^* . Curves are generated using the split sum for $L_d = 50, 100, 200, 300, 400, 500, 600, 700, 800, 900$ and 1000 km.

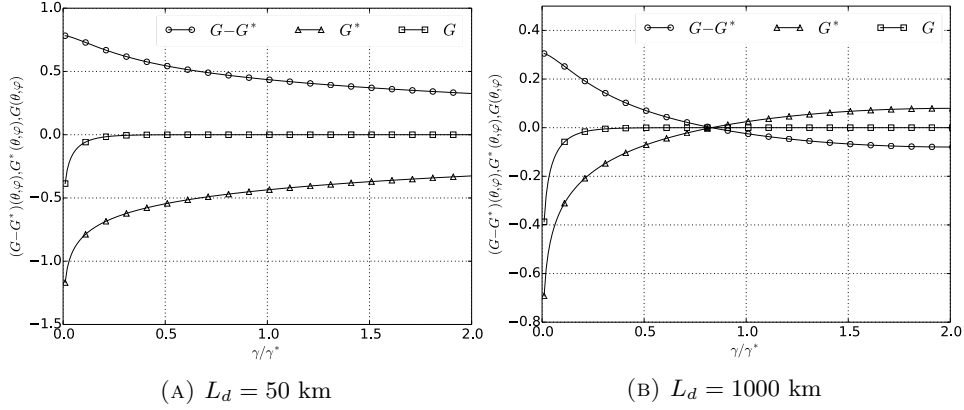


FIGURE 4. $(G - G^*)$, G^* and G vs. γ/γ^* for (a) $L_d = 50$ km, (b) $L_d = 100$ km. Curves are generated using the split sum.

8. ACKNOWLEDGMENTS

This work is supported by the University Research Board of the American University of Beirut. The authors would like to acknowledge Professor Leila Issa of the Lebanese American University-Beirut for her insightful feedback on the mathematical derivation of the convergence of the Green's Function.

9. APPENDIX

In this section, we present tables of the values of the Green's function versus γ/γ^* , for values of the screening constant L_d of 50, 100, 200, 400, 800, 1000 km.

TABLE 3. $G(\theta, \varphi)$ function of γ/γ^* for $L_d = 50, 100, 200$ km. The values presented are computed using the split sum. The stopping criteria used is when the term contribution of $G(l)$ to the split sum drops down below 1E-20.

$10\gamma/\gamma^*$	$G(\theta, \varphi), L_d = 50$ km	$G(\theta, \varphi), L_d = 100$ km	$G(\theta, \varphi), L_d = 200$ km
1	-0.386281669	-0.386286557	-0.386306107
2	-0.278953105	-0.278957963	-0.278977364
3	-0.218435407	-0.218440190	-0.218459383
4	-0.177384391	-0.177389115	-0.177407995
5	-0.147127405	-0.147132024	-0.147150531
6	-0.123747990	-0.123752505	-0.123770580
7	-0.105126463	-0.105130859	-0.105148457
8	-8.99792090E-02	-8.99834707E-02	-9.00005400E-02
9	-7.74669051E-02	-7.74710327E-02	-7.74875507E-02
10	-6.70094490E-02	-6.70134276E-02	-6.70293644E-02
11	-5.81887029E-02	-5.81925362E-02	-5.82078733E-02
12	-5.06933816E-02	-5.06970622E-02	-5.07117920E-02
13	-4.42856625E-02	-4.42891903E-02	-4.43033017E-02
14	-3.87800299E-02	-3.87834013E-02	-3.87968980E-02
15	-3.40292826E-02	-3.40325013E-02	-3.40453833E-02
16	-2.99149491E-02	-2.99180150E-02	-2.99302880E-02
17	-2.63405293E-02	-2.63434462E-02	-2.63551176E-02
18	-2.32266262E-02	-2.32293960E-02	-2.32404824E-02
19	-2.05073487E-02	-2.05099769E-02	-2.05204897E-02
20	-1.81276016E-02	-1.81300901E-02	-1.81400459E-02
21	-1.60410143E-02	-1.60433669E-02	-1.60527844E-02
22	-1.42083438E-02	-1.42105669E-02	-1.42194629E-02
23	-1.25962095E-02	-1.25983069E-02	-1.26067009E-02
24	-1.11760953E-02	-1.11780716E-02	-1.11859832E-02
25	-9.92354099E-03	-9.92540177E-03	-9.93285049E-03
26	-8.81749671E-03	-8.81924666E-03	-8.82625207E-03
27	-7.83978775E-03	-7.84143247E-03	-7.84801599E-03
28	-6.97468081E-03	-6.97622448E-03	-6.98240474E-03
29	-6.20851712E-03	-6.20996533E-03	-6.21576235E-03
30	-5.52941579E-03	-5.53077273E-03	-5.53620607E-03
31	-4.92701819E-03	-4.92828898E-03	-4.93337726E-03
32	-4.39227652E-03	-4.39346535E-03	-4.39822720E-03
33	-3.91727407E-03	-3.91838606E-03	-3.92283872E-03
34	-3.49507318E-03	-3.49611230E-03	-3.50027299E-03
35	-3.11958441E-03	-3.12055484E-03	-3.12444032E-03
36	-2.78545590E-03	-2.78636138E-03	-2.78998748E-03
37	-2.48797797E-03	-2.48882244E-03	-2.49220454E-03

Table 3 continued from previous page

$10\gamma/\gamma^*$	$G(\theta, \varphi), L_d = 50 \text{ km}$	$G(\theta, \varphi), L_d = 100 \text{ km}$	$G(\theta, \varphi), L_d = 200 \text{ km}$
38	-2.22300179E-03	-2.22378876E-03	-2.22694129E-03
39	-1.98686752E-03	-1.98760070E-03	-1.99053762E-03
40	-1.77634496E-03	-1.77702762E-03	-1.77976210E-03
41	-1.58857903E-03	-1.58921431E-03	-1.59175904E-03
42	-1.42104481E-03	-1.42163562E-03	-1.42400258E-03
43	-1.27150724E-03	-1.27205648E-03	-1.27425697E-03
44	-1.13798620E-03	-1.13849656E-03	-1.14054140E-03
45	-1.01872673E-03	-1.01920078E-03	-1.02109998E-03
46	-9.12171672E-04	-9.12611722E-04	-9.14375007E-04
47	-8.16938817E-04	-8.17347143E-04	-8.18983535E-04
48	-7.31800625E-04	-7.32179382E-04	-7.33697321E-04
49	-6.55665994E-04	-6.56017161E-04	-6.57424738E-04
50	-5.87564951E-04	-5.87890449E-04	-5.89195115E-04
51	-5.26634336E-04	-5.26935910E-04	-5.28144767E-04
52	-4.72106069E-04	-4.72385378E-04	-4.73505061E-04
53	-4.23296093E-04	-4.23554680E-04	-4.24591417E-04
54	-3.79595032E-04	-3.79834353E-04	-3.80793936E-04
55	-3.40459781E-04	-3.40681203E-04	-3.41569073E-04
56	-3.05406109E-04	-3.05610913E-04	-3.06432194E-04
57	-2.74002145E-04	-2.74191494E-04	-2.74950959E-04
58	-2.45862553E-04	-2.46037584E-04	-2.46739626E-04
59	-2.20643400E-04	-2.20805145E-04	-2.21453927E-04
60	-1.98037596E-04	-1.98187015E-04	-1.98786423E-04
61	-1.77770882E-04	-1.77908878E-04	-1.78462506E-04
62	-1.59598261E-04	-1.59725663E-04	-1.60236872E-04
63	-1.43300756E-04	-1.43418350E-04	-1.43890255E-04
64	-1.28682659E-04	-1.28791173E-04	-1.29226697E-04
65	-1.15568961E-04	-1.15669085E-04	-1.16070922E-04
66	-1.03803170E-04	-1.03895516E-04	-1.04266182E-04
67	-9.32452676E-05	-9.33304182E-05	-9.36722572E-05
68	-8.37699772E-05	-8.38484848E-05	-8.41636574E-05
69	-7.52651904E-05	-7.53375498E-05	-7.56280788E-05
70	-6.76305353E-05	-6.76972195E-05	-6.79649602E-05
71	-6.07761576E-05	-6.08375885E-05	-6.10842908E-05
72	-5.46215779E-05	-5.46781630E-05	-5.49054203E-05
73	-4.90947168E-05	-4.91468236E-05	-4.93561311E-05
74	-4.41309930E-05	-4.41789707E-05	-4.43717036E-05
75	-3.96725482E-05	-3.97167169E-05	-3.98941556E-05
76	-3.56675264E-05	-3.57081772E-05	-3.58715042E-05
77	-3.20694453E-05	-3.21068510E-05	-3.22571577E-05
78	-2.88366336E-05	-2.88710471E-05	-2.90093503E-05
79	-2.59317294E-05	-2.59633835E-05	-2.60906163E-05
80	-2.33212249E-05	-2.33503379E-05	-2.34673662E-05
81	-2.09750706E-05	-2.10018407E-05	-2.11094648E-05
82	-1.88663071E-05	-1.88909180E-05	-1.89898783E-05

Table 3 continued from previous page

$10\gamma/\gamma^*$	$G(\theta, \varphi), L_d = 50 \text{ km}$	$G(\theta, \varphi), L_d = 100 \text{ km}$	$G(\theta, \varphi), L_d = 200 \text{ km}$
83	-1.69707491E-05	-1.69933737E-05	-1.70843505E-05
84	-1.52666980E-05	-1.52874909E-05	-1.53711153E-05
85	-1.37346760E-05	-1.37537836E-05	-1.38306377E-05
86	-1.23572072E-05	-1.23747632E-05	-1.24453845E-05
87	-1.11186018E-05	-1.11347299E-05	-1.11996142E-05
88	-1.00047755E-05	-1.00195894E-05	-1.00791931E-05
89	-9.00308260E-06	-9.01668682E-06	-9.07143294E-06
90	-8.10216807E-06	-8.11465998E-06	-8.16493684E-06
91	-7.29183557E-06	-7.30330430E-06	-7.34947025E-06
92	-6.56292559E-06	-6.57345345E-06	-6.61583863E-06
93	-5.90721220E-06	-5.91687558E-06	-5.95578467E-06
94	-5.31730620E-06	-5.32617469E-06	-5.36188782E-06
95	-4.78656784E-06	-4.79470600E-06	-4.82748146E-06
96	-4.30903310E-06	-4.31649960E-06	-4.34657522E-06
97	-3.87934051E-06	-3.88619037E-06	-3.91378535E-06
98	-3.49267475E-06	-3.49895777E-06	-3.52427310E-06
99	-3.14470549E-06	-3.15046805E-06	-3.17368972E-06
100	-2.83154236E-06	-2.83682698E-06	-2.85812553E-06
101	-2.54968745E-06	-2.55453324E-06	-2.57406555E-06
102	-2.29599664E-06	-2.30043929E-06	-2.31834997E-06
103	-2.06764298E-06	-2.07171570E-06	-2.08813753E-06
104	-1.86208513E-06	-1.86581826E-06	-1.88087324E-06
105	-1.67703740E-06	-1.68045904E-06	-1.69425948E-06
106	-1.51044492E-06	-1.51358063E-06	-1.52622977E-06
107	-1.36045946E-06	-1.36333290E-06	-1.37492543E-06
108	-1.22541883E-06	-1.22805159E-06	-1.23867483E-06
109	-1.10382803E-06	-1.10623989E-06	-1.11597399E-06
110	-9.94342145E-07	-9.96551535E-07	-1.00546993E-06
111	-8.95751498E-07	-8.97775294E-07	-9.05945456E-07
112	-8.06967819E-07	-8.08821312E-07	-8.16305430E-07
113	-7.27011923E-07	-7.28709381E-07	-7.35564299E-07
114	-6.55002964E-07	-6.56557290E-07	-6.62835419E-07
115	-5.90148204E-07	-5.91571393E-07	-5.97320707E-07
116	-5.31734372E-07	-5.33037337E-07	-5.38301890E-07
117	-4.79119592E-07	-4.80312451E-07	-4.85132716E-07
118	-4.31726249E-07	-4.32818126E-07	-4.37231193E-07
119	-3.89034426E-07	-3.90033819E-07	-3.94073737E-07
120	-3.50576187E-07	-3.51490826E-07	-3.55188860E-07
121	-3.15930350E-07	-3.16767370E-07	-3.20152168E-07
122	-2.84717800E-07	-2.85483736E-07	-2.88581560E-07
123	-2.56597247E-07	-2.57298069E-07	-2.60133021E-07
124	-2.31261438E-07	-2.31902618E-07	-2.34496824E-07
125	-2.08433789E-07	-2.09020371E-07	-2.11394052E-07
126	-1.87865254E-07	-1.88401842E-07	-1.90573601E-07
127	-1.69331628E-07	-1.69822428E-07	-1.71809290E-07

Table 3 continued from previous page

$10\gamma/\gamma^*$	$G(\theta, \varphi), L_d = 50 \text{ km}$	$G(\theta, \varphi), L_d = 100 \text{ km}$	$G(\theta, \varphi), L_d = 200 \text{ km}$
128	-1.52630975E-07	-1.53079881E-07	-1.54897435E-07
129	-1.37581523E-07	-1.37992075E-07	-1.39654645E-07
130	-1.24019579E-07	-1.24395001E-07	-1.25915690E-07
131	-1.11797668E-07	-1.12140981E-07	-1.13531790E-07
132	-1.00783062E-07	-1.01096965E-07	-1.02368901E-07
133	-9.08561688E-08	-9.11431712E-08	-9.23063155E-08
134	-8.19092989E-08	-8.21716881E-08	-8.32352640E-08
135	-7.38454560E-08	-7.40853068E-08	-7.50577840E-08
136	-6.65772504E-08	-6.67965026E-08	-6.76856118E-08
137	-6.00259824E-08	-6.02263910E-08	-6.10392377E-08
138	-5.41207683E-08	-5.43039427E-08	-5.50470141E-08
139	-4.87977516E-08	-4.89651484E-08	-4.96443917E-08
140	-4.39993748E-08	-4.41523511E-08	-4.47732091E-08
141	-3.96738145E-08	-3.98136066E-08	-4.03810603E-08
142	-3.57743737E-08	-3.59021080E-08	-3.64207224E-08
143	-3.22589777E-08	-3.23756879E-08	-3.28496341E-08
144	-2.90897102E-08	-2.91963431E-08	-2.96294473E-08
145	-2.62324260E-08	-2.63298432E-08	-2.67255995E-08
146	-2.36563462E-08	-2.37453328E-08	-2.41069404E-08
147	-2.13337188E-08	-2.14150138E-08	-2.17453984E-08
148	-1.92395699E-08	-1.93138252E-08	-1.96156691E-08
149	-1.73513719E-08	-1.74191932E-08	-1.76949460E-08
150	-1.56488333E-08	-1.57107714E-08	-1.59626712E-08
151	-1.41136454E-08	-1.41702143E-08	-1.44003156E-08
152	-1.27293438E-08	-1.27809985E-08	-1.29911744E-08
153	-1.14810517E-08	-1.15282264E-08	-1.17201910E-08
154	-1.03553974E-08	-1.03984670E-08	-1.05737916E-08
155	-9.34028943E-09	-9.37961975E-09	-9.53973700E-09
156	-8.42486525E-09	-8.46077342E-09	-8.60699600E-09
157	-7.59931229E-09	-7.63209584E-09	-7.76562104E-09
158	-6.85479051E-09	-6.88471902E-09	-7.00664504E-09
159	-6.18333251E-09	-6.21065332E-09	-6.32198160E-09
160	-5.57775426E-09	-5.60269475E-09	-5.70434011E-09
161	-5.03158537E-09	-5.05434494E-09	-5.14714760E-09
162	-4.53897409E-09	-4.55975213E-09	-4.64447547E-09
163	-4.09467127E-09	-4.11363610E-09	-4.19097956E-09
164	-3.69393183E-09	-3.71123487E-09	-3.78183973E-09
165	-3.33246919E-09	-3.34826056E-09	-3.41270923E-09
166	-3.00642644E-09	-3.02084047E-09	-3.07966852E-09
167	-2.71233902E-09	-2.72548850E-09	-2.77918244E-09
168	-2.44705856E-09	-2.45905718E-09	-2.50806331E-09
169	-2.20776197E-09	-2.21870988E-09	-2.26343566E-09
170	-1.99189643E-09	-2.00188843E-09	-2.04270645E-09
171	-1.79717496E-09	-1.80628723E-09	-1.84353699E-09
172	-1.62151270E-09	-1.62982572E-09	-1.66381753E-09

Table 3 continued from previous page

$10\gamma/\gamma^*$	$G(\theta, \varphi), L_d = 50 \text{ km}$	$G(\theta, \varphi), L_d = 100 \text{ km}$	$G(\theta, \varphi), L_d = 200 \text{ km}$
173	-1.46304457E-09	-1.47062817E-09	-1.50164581E-09
174	-1.32008116E-09	-1.32700273E-09	-1.35530509E-09
175	-1.19111354E-09	-1.19742449E-09	-1.22324773E-09
176	-1.07475628E-09	-1.08051634E-09	-1.10407716E-09
177	-9.69787584E-10	-9.75037384E-10	-9.96533633E-10
178	-8.75078177E-10	-8.79870343E-10	-8.99481212E-10
179	-7.89633137E-10	-7.94003419E-10	-8.11894552E-10
180	-7.12542081E-10	-7.16527948E-10	-7.32849004E-10
181	-6.42990494E-10	-6.46622145E-10	-6.61510458E-10
182	-5.80230419E-10	-5.83545989E-10	-5.97126126E-10
183	-5.23609933E-10	-5.26629684E-10	-5.39017220E-10
184	-4.72515582E-10	-4.75272321E-10	-4.86571061E-10
185	-4.26419122E-10	-4.28929697E-10	-4.39235009E-10
186	-3.84819399E-10	-3.87111510E-10	-3.96510380E-10
187	-3.47288559E-10	-3.49375445E-10	-3.57947338E-10
188	-3.13416904E-10	-3.15322934E-10	-3.23139737E-10
189	-2.82855184E-10	-2.84593071E-10	-2.91721508E-10
190	-2.55280103E-10	-2.56861588E-10	-2.63362082E-10
191	-2.30390998E-10	-2.31835107E-10	-2.37763254E-10
192	-2.07933740E-10	-2.09250714E-10	-2.14655807E-10
193	-1.87667978E-10	-1.88868629E-10	-1.93797103E-10
194	-1.69382397E-10	-1.70473691E-10	-1.74967846E-10
195	-1.52878210E-10	-1.53873220E-10	-1.57970317E-10
196	-1.37981140E-10	-1.38890732E-10	-1.42626216E-10
197	-1.24539587E-10	-1.25368757E-10	-1.28774297E-10
198	-1.12408867E-10	-1.13164270E-10	-1.16269397E-10
199	-1.01460999E-10	-1.02149539E-10	-1.04980309E-10
200	-9.15805209E-11	-9.22080745E-11	-9.47886630E-11

TABLE 4. $G(\theta, \varphi)$ function of γ/γ^* for $L_d = 400, 800, 1000$ km. The values presented are computed using the split sum. The stopping critera used is when the term contribution of $G(l)$ to the split sum drops down below 1E-20.

$10\gamma/\gamma^*$	$G(\theta, \varphi), L_d = 400$ km	$G(\theta, \varphi), L_d = 800$ km	$G(\theta, \varphi), L_d = 1000$ km
1	-0.386384428	-0.386698574	-0.386935174
2	-0.279055119	-0.279367000	-0.279601902
3	-0.218536198	-0.218844444	-0.219076619
4	-0.177483588	-0.177786931	-0.178015471
5	-0.147224635	-0.147522002	-0.147746071
6	-0.123842940	-0.124133401	-0.124352314
7	-0.105218887	-0.105501644	-0.105714813
8	-9.00688842E-02	-9.03433040E-02	-9.05502513E-02
9	-7.75536671E-02	-7.78192431E-02	-7.80195743E-02
10	-6.70931637E-02	-6.73494935E-02	-6.75429255E-02
11	-5.82692884E-02	-5.85160889E-02	-5.87023981E-02
12	-5.07707670E-02	-5.10078520E-02	-5.11869080E-02
13	-4.43598181E-02	-4.45870832E-02	-4.47588041E-02
14	-3.88509482E-02	-3.90683748E-02	-3.92327383E-02
15	-3.40969786E-02	-3.43046039E-02	-3.44616435E-02
16	-2.99794525E-02	-3.01773753E-02	-3.03271618E-02
17	-2.64018904E-02	-2.65902579E-02	-2.67328992E-02
18	-2.32849084E-02	-2.34639104E-02	-2.35995445E-02
19	-2.05626264E-02	-2.07324829E-02	-2.08612736E-02
20	-1.81799550E-02	-1.83409173E-02	-1.84630472E-02
21	-1.60905365E-02	-1.62428729E-02	-1.63585451E-02
22	-1.42551288E-02	-1.43991308E-02	-1.45085575E-02
23	-1.26403589E-02	-1.27763264E-02	-1.28797302E-02
24	-1.12177096E-02	-1.13459527E-02	-1.14435637E-02
25	-9.96272545E-03	-1.00835599E-02	-1.01756109E-02
26	-8.85435659E-03	-8.96809902E-03	-9.05482657E-03
27	-7.87442829E-03	-7.98139721E-03	-8.06303602E-03
28	-7.00720632E-03	-7.10771605E-03	-7.18449941E-03
29	-6.23903004E-03	-6.33339258E-03	-6.40555192E-03
30	-5.55801764E-03	-5.64653799E-03	-5.71429962E-03
31	-4.95380722E-03	-5.03678387E-03	-5.10037038E-03
32	-4.41734865E-03	-4.49507311E-03	-4.55470011E-03
33	-3.94072337E-03	-4.01347689E-03	-4.06935439E-03
34	-3.51698906E-03	-3.58504499E-03	-3.63737578E-03
35	-3.14005348E-03	-3.20367469E-03	-3.25265480E-03
36	-2.80456175E-03	-2.86400085E-03	-2.90981843E-03
37	-2.50580069E-03	-2.56130029E-03	-2.60413601E-03
38	-2.23961752E-03	-2.29141000E-03	-2.33143684E-03
39	-2.00234959E-03	-2.05065659E-03	-2.08804011E-03
40	-1.79076288E-03	-1.83579559E-03	-1.87069364E-03
41	-1.60199881E-03	-1.64395850E-03	-1.67652150E-03

Table 4 continued from previous page

$10\gamma/\gamma^*$	$G(\theta, \varphi), L_d = 400 \text{ km}$	$G(\theta, \varphi), L_d = 800 \text{ km}$	$G(\theta, \varphi), L_d = 1000 \text{ km}$
42	-1.43352943E-03	-1.47260714E-03	-1.50297780E-03
43	-1.28311617E-03	-1.31949317E-03	-1.34780735E-03
44	-1.14877592E-03	-1.18262402E-03	-1.20901014E-03
45	-1.02875044E-03	-1.06023205E-03	-1.08481187E-03
46	-9.21479717E-04	-9.50748275E-04	-9.73636983E-04
47	-8.25578638E-04	-8.52779020E-04	-8.74085352E-04
48	-7.39816925E-04	-7.65085628E-04	-7.84912205E-04
49	-6.63100916E-04	-6.86566520E-04	-7.05009967E-04
50	-5.94457961E-04	-6.16241363E-04	-6.33392832E-04
51	-5.33022627E-04	-5.53237507E-04	-5.69182623E-04
52	-4.78024449E-04	-4.96777589E-04	-5.11596852E-04
53	-4.28777217E-04	-4.46168735E-04	-4.59937815E-04
54	-3.84669518E-04	-4.00793273E-04	-4.13583126E-04
55	-3.45156266E-04	-3.60100210E-04	-3.71977425E-04
56	-3.09751369E-04	-3.23597807E-04	-3.34624754E-04
57	-2.78021209E-04	-2.90847180E-04	-3.01082298E-04
58	-2.49578821E-04	-2.61456298E-04	-2.70954217E-04
59	-2.24078656E-04	-2.35074913E-04	-2.43886810E-04
60	-2.01212213E-04	-2.11390012E-04	-2.19563706E-04
61	-1.80703821E-04	-1.90121791E-04	-1.97701956E-04
62	-1.62307202E-04	-1.71019958E-04	-1.78048329E-04
63	-1.45802158E-04	-1.53860659E-04	-1.60376163E-04
64	-1.30991830E-04	-1.38443531E-04	-1.44482517E-04
65	-1.17700161E-04	-1.24589249E-04	-1.30185595E-04
66	-1.05769635E-04	-1.12137255E-04	-1.17322532E-04
67	-9.50593094E-05	-1.00943726E-04	-1.05747371E-04
68	-8.54430400E-05	-9.08798320E-05	-9.53292547E-05
69	-7.68078753E-05	-8.18301341E-05	-8.59508509E-05
70	-6.90527013E-05	-7.36911607E-05	-7.75069275E-05
71	-6.20869396E-05	-6.63701576E-05	-6.99030570E-05
72	-5.58294523E-05	-5.97839353E-05	-6.30545183E-05
73	-5.02075345E-05	-5.38578897E-05	-5.68852702E-05
74	-4.51560409E-05	-4.85250930E-05	-5.13270279E-05
75	-4.06165636E-05	-4.37254967E-05	-4.63184842E-05
76	-3.65367523E-05	-3.94051967E-05	-4.18045638E-05
77	-3.28696624E-05	-3.55158154E-05	-3.77358010E-05
78	-2.95731879E-05	-3.20139188E-05	-3.40677325E-05
79	-2.66095667E-05	-2.88605006E-05	-3.07604096E-05
80	-2.39449200E-05	-2.60205252E-05	-2.77779127E-05
81	-2.15488508E-05	-2.34625259E-05	-2.50879511E-05
82	-1.93940832E-05	-2.11582283E-05	-2.26614848E-05
83	-1.74561319E-05	-1.90822248E-05	-2.04723947E-05
84	-1.57130198E-05	-1.72116779E-05	-1.84971850E-05
85	-1.41450209E-05	-1.55260641E-05	-1.67147118E-05
86	-1.27344174E-05	-1.40069278E-05	-1.51059503E-05

Table 4 continued from previous page

$10\gamma/\gamma^*$	$G(\theta, \varphi), L_d = 400 \text{ km}$	$G(\theta, \varphi), L_d = 800 \text{ km}$	$G(\theta, \varphi), L_d = 1000 \text{ km}$
87	-1.14653030E-05	-1.26376763E-05	-1.36537765E-05
88	-1.03233888E-05	-1.14033865E-05	-1.23427744E-05
89	-9.29584166E-06	-1.02906370E-05	-1.11590643E-05
90	-8.37113475E-06	-9.28735335E-06	-1.00901480E-05
91	-7.53890936E-06	-8.38267351E-06	-9.12476662E-06
92	-6.78985862E-06	-7.56682175E-06	-8.25278130E-06
93	-6.11561973E-06	-6.83100325E-06	-7.46505657E-06
94	-5.50867571E-06	-6.16729949E-06	-6.75335968E-06
95	-4.96227085E-06	-5.56858458E-06	-6.11027281E-06
96	-4.47033199E-06	-5.02844159E-06	-5.52910888E-06
97	-4.02739897E-06	-4.54109431E-06	-5.00384112E-06
98	-3.62856304E-06	-4.10134044E-06	-4.52903441E-06
99	-3.26941017E-06	-3.70449447E-06	-4.09978884E-06
100	-2.94597044E-06	-3.34633683E-06	-3.71168539E-06
101	-2.65467452E-06	-3.02306603E-06	-3.36073822E-06
102	-2.39231076E-06	-2.73125738E-06	-3.04335163E-06
103	-2.15599152E-06	-2.46782497E-06	-2.75628190E-06
104	-1.94311815E-06	-2.22998847E-06	-2.49660184E-06
105	-1.75135312E-06	-2.01524199E-06	-2.26167026E-06
106	-1.57859324E-06	-1.82132658E-06	-2.04910316E-06
107	-1.42294596E-06	-1.64620656E-06	-1.85674855E-06
108	-1.28270835E-06	-1.48804668E-06	-1.68266388E-06
109	-1.15634771E-06	-1.34519212E-06	-1.52509517E-06
110	-1.04248466E-06	-1.21615074E-06	-1.38245855E-06
111	-9.39877509E-07	-1.09957716E-06	-1.25332360E-06
112	-8.47408728E-07	-9.94258130E-07	-1.13639840E-06
113	-7.64072240E-07	-8.99099007E-07	-1.03051593E-06
114	-6.88962245E-07	-8.13112649E-07	-9.34621937E-07
115	-6.21263268E-07	-7.35408548E-07	-8.47763715E-07
116	-5.60241062E-07	-6.65183222E-07	-7.69080543E-07
117	-5.05234368E-07	-6.01711747E-07	-6.97794405E-07
118	-4.55647807E-07	-5.44339969E-07	-6.33202205E-07
119	-4.10945205E-07	-4.92477454E-07	-5.74668263E-07
120	-3.70643619E-07	-4.45591553E-07	-5.21617949E-07
121	-3.34308112E-07	-4.03201284E-07	-4.73531713E-07
122	-3.01546834E-07	-3.64872591E-07	-4.29939774E-07
123	-2.72006929E-07	-3.30213538E-07	-3.90417199E-07
124	-2.45370416E-07	-2.98870390E-07	-3.54579697E-07
125	-2.21350916E-07	-2.70523657E-07	-3.22079671E-07
126	-1.99690348E-07	-2.44884887E-07	-2.92602635E-07
127	-1.80156249E-07	-2.21693597E-07	-2.65864031E-07
128	-1.62539081E-07	-2.00714510E-07	-2.41606443E-07
129	-1.46650109E-07	-1.81735132E-07	-2.19596799E-07
130	-1.32319187E-07	-1.64563517E-07	-1.99624267E-07
131	-1.19393036E-07	-1.49026292E-07	-1.81497953E-07

Table 4 continued from previous page

$10\gamma/\gamma^*$	$G(\theta, \varphi), L_d = 400 \text{ km}$	$G(\theta, \varphi), L_d = 800 \text{ km}$	$G(\theta, \varphi), L_d = 1000 \text{ km}$
132	-1.07733470E-07	-1.34966811E-07	-1.65045066E-07
133	-9.72159810E-08	-1.22243534E-07	-1.50109145E-07
134	-8.77283313E-08	-1.10728593E-07	-1.36548522E-07
135	-7.91693537E-08	-1.00306416E-07	-1.24234930E-07
136	-7.14478503E-08	-9.08725823E-08	-1.13052174E-07
137	-6.44816183E-08	-8.23327042E-08	-1.02895029E-07
138	-5.81965480E-08	-7.46014734E-08	-9.36681559E-08
139	-5.25258272E-08	-6.76017820E-08	-8.52851940E-08
140	-4.74092232E-08	-6.12639113E-08	-7.76678917E-08
141	-4.27924221E-08	-5.55248469E-08	-7.07453296E-08
142	-3.86264531E-08	-5.03276070E-08	-6.44532392E-08
143	-3.48671669E-08	-4.56206770E-08	-5.87333808E-08
144	-3.14747375E-08	-4.13574632E-08	-5.35329470E-08
145	-2.84132664E-08	-3.74958411E-08	-4.88040683E-08
146	-2.56503689E-08	-3.39976971E-08	-4.45033486E-08
147	-2.31568436E-08	-3.08285770E-08	-4.05914271E-08
148	-2.09063540E-08	-2.79573058E-08	-3.70326099E-08
149	-1.88751450E-08	-2.53556820E-08	-3.37945316E-08
150	-1.70417902E-08	-2.29981953E-08	-3.08478256E-08
151	-1.53869646E-08	-2.08617656E-08	-2.81658483E-08
152	-1.38932359E-08	-1.89255083E-08	-2.57244359E-08
153	-1.25448789E-08	-1.71705263E-08	-2.35016540E-08
154	-1.13277068E-08	-1.55797206E-08	-2.14776001E-08
155	-1.02289244E-08	-1.41376129E-08	-1.96342125E-08
156	-9.23698362E-09	-1.28301973E-08	-1.79550899E-08
157	-8.34146974E-09	-1.16447962E-08	-1.64253517E-08
158	-7.53298401E-09	-1.05699325E-08	-1.50314801E-08
159	-6.80304790E-09	-9.59521707E-09	-1.37612064E-08
160	-6.14400975E-09	-8.71124506E-09	-1.26033859E-08
161	-5.54896618E-09	-7.90949883E-09	-1.15478977E-08
162	-5.01168707E-09	-7.18226900E-09	-1.05855493E-08
163	-4.52655158E-09	-6.52257182E-09	-9.70799086E-09
164	-4.08848599E-09	-5.92408433E-09	-8.90763641E-09
165	-3.69291242E-09	-5.38107958E-09	-8.17759194E-09
166	-3.33569927E-09	-4.88837015E-09	-7.51159668E-09
167	-3.01311731E-09	-4.44125758E-09	-6.90395785E-09
168	-2.72180123E-09	-4.03548572E-09	-6.34950403E-09
169	-2.45871346E-09	-3.66719832E-09	-5.84353499E-09
170	-2.22111218E-09	-3.33290218E-09	-5.38177947E-09
171	-2.00652250E-09	-3.02943159E-09	-4.96035346E-09
172	-1.81271054E-09	-2.75391820E-09	-4.57572913E-09
173	-1.63766012E-09	-2.50376275E-09	-4.22469837E-09
174	-1.47955059E-09	-2.27660957E-09	-3.90434662E-09
175	-1.33673883E-09	-2.07032347E-09	-3.61202490E-09
176	-1.20774146E-09	-1.88296911E-09	-3.34532624E-09

Table 4 continued from previous page

$10\gamma/\gamma^*$	$G(\theta, \varphi), L_d = 400 \text{ km}$	$G(\theta, \varphi), L_d = 800 \text{ km}$	$G(\theta, \varphi), L_d = 1000 \text{ km}$
177	-1.09121912E-09	-1.71279202E-09	-3.10206394E-09
178	-9.85962534E-10	-1.55820190E-09	-2.88025204E-09
179	-8.90880258E-10	-1.41775669E-09	-2.67808775E-09
180	-8.04986577E-10	-1.29014888E-09	-2.49393417E-09
181	-7.27391591E-10	-1.17419319E-09	-2.32630715E-09
182	-6.57291721E-10	-1.06881426E-09	-2.17386131E-09
183	-5.93961436E-10	-9.73037095E-10	-2.03537787E-09
184	-5.36745648E-10	-8.85977292E-10	-1.90975413E-09
185	-4.85052665E-10	-8.06832823E-10	-1.79599446E-09
186	-4.38348247E-10	-7.34875882E-10	-1.69320002E-09
187	-3.96150029E-10	-6.69446276E-10	-1.60056179E-09
188	-3.58022251E-10	-6.09945150E-10	-1.51735369E-09
189	-3.23571503E-10	-5.55828938E-10	-1.44292556E-09
190	-2.92442404E-10	-5.06604481E-10	-1.37669776E-09
191	-2.64314043E-10	-4.61824246E-10	-1.31815625E-09
192	-2.38896541E-10	-4.21081975E-10	-1.26684785E-09
193	-2.15928109E-10	-3.84008964E-10	-1.22237653E-09
194	-1.95172295E-10	-3.50270563E-10	-1.18439991E-09
195	-1.76415521E-10	-3.19562904E-10	-1.15262611E-09
196	-1.59464858E-10	-2.91610125E-10	-1.12681164E-09
197	-1.44146042E-10	-2.66161732E-10	-1.10675868E-09
198	-1.30301672E-10	-2.42990295E-10	-1.09231402E-09
199	-1.17789528E-10	-2.21889243E-10	-1.08336740E-09
200	-1.06481164E-10	-2.02670977E-10	-1.07985043E-09

REFERENCES

1. V. A. Bogomolov, *Dynamics of vorticity at a sphere*, Fluid Dynamics **12** (1977), no. 6, 863–870.
2. Peter Bosler, Lei Wang, Christiane Jablonowski, and Robert Krasny, *A lagrangian particle/panel method for the barotropic vorticity equations on a rotating sphere*, Fluid Dynamics Research **46** (2014), no. 3, 031406.
3. Dudley B. Chelton, Roland A. deSzoeke, Michael G. Schlax, Karim El Naggar, and Nicolas Siwertz, *Geographical Variability of the First Baroclinic Rossby Radius of Deformation*, J. Phys. Oceanogr. **28** (1998), no. 3, 433–460.
4. Willi Freeden and Michael Schreiner, *Spherical functions of mathematical geosciences*, Springer, Verlag Berlin Heidelberg, 2009 (English).
5. Adrian E. Gill, *Atmosphere-ocean dynamics*, International Geophysics Series, vol. 30, Academic Press, 1982.
6. I. S. Gradshteyn and I. M. Ryzhik, *Table of integrals, series, and products*, 8th ed., Elsevier, 2015.
7. Yoshifumi Kimura and Hisashi Okamoto, *Vortex motion on a sphere*, Journal of the Physical Society of Japan **56** (1987), no. 12, 4203–4206.
8. A. Mohammadian and John Marshall, *A “vortex in cel” model for quasi-geostrophic, shallow water dynamics on the sphere*, Ocean Modelling **32** (2010), no. 3, 132–142 (English).
9. Joseph Pedlosky, *Geophysical fluid dynamics*, 2nd ed., Springer, New York, 1987 (English).
10. G. K. Vallis, *Atmospheric and oceanic fluid dynamics*, Cambridge University Press, Cambridge, U.K., 2006.

AMERICAN UNIVERSITY OF BEIRUT, BEIRUT, LEBANON

Current address: xxx

E-mail address: rgt09@mail.aub.edu

AMERICAN UNIVERSITY OF BEIRUT, BEIRUT, LEBANON

Current address: King Abdullah University of Science and Technology, Thuwal 23955, Saudi Arabia

E-mail address: Samah.Mohtar@kaust.edu.sa

DUKE UNIVERSITY, DURHAM, NC 27708, USA

Current address: King Abdullah University of Science and Technology, Thuwal 23955, Saudi Arabia

E-mail address: Omar.Knio@kaust.edu.sa

AMERICAN UNIVERSITY OF BEIRUT, BEIRUT, LEBANON

E-mail address: issam.lakkis@aub.du.lb